Compañ Moreno, V.; Escorihuela Fuentes, J.; Olvera, J.; Garcia-Bernabe, A.; Andrio, A. (2020). Influence of the anion on diffusivity and mobility of ionic liquids composite polybenzimidazol membranes. Electrochimica Acta. 354:1-12. https://doi.org/10.1016/j.electacta.2020.136666

Influence of the anion on diffusivity and mobility of ionic liquids composite polybenzimidazol membranes

Vicente Compañ,*[†] *Jorge Escorihuela,*[‡] *Jessica Olvera,*[§] *Abel García-Bernabé,* [†] *and Andreu Andrio,*[‖]

† Departamento de Termodinámica Aplicada, Universitat Politècnica de València, Camino de Vera s/n, 46020 Valencia, Spain. ‡ Departament de Química Orgànica, Facultat de Farmàcia, Universitat de València, Av. Vicent Andrés Estellés s/n, 46100, Burjassot, Valencia, Spain. § Departamento de Polímeros del Instituto de Investigación en Materiales de la Universidad Autónoma de México (UNAM).‖ Departamento de Física Aplicada, Universitat Jaume I, Avda. Sos Baynat, s/n, 12080, Castelló de la Plana, Spain

KEYWORDS: polymer electrolytes; polybenzimidazole; ionic liquids; conductivity, ionic transport; mobility, electrochemical impedance spectroscopy.

ABSTRACT

The study of proton conductivity processes has received intensive attention in the past decades due to their potential applications in fields such as electrochemical devices and fuel cells. Despite the high number of composite membranes which have been described for this purpose, fundamental studies of the conduction phenomena in polymeric membranes are scarce. In this report, we study on the effect of the anion on ionic conductivity of ionic liquid composite polybenzimidazole (PBI) membranes. These membranes, which contain 1-butyl-3-methylimidazolium (BMIM) with different counterions ($[Cl]^-$, $[NCS]^-$, $[NTf_2]^-$ and $[BF_4]^-$), were analyzed by electrochemical impedance spectroscopy (EIS) in order to study the influence of the anion on the conductivity, but also mobility and charge carrier density at different temperatures. The methodology for this analysis of the is based on the Coelho model of electrode polarization (EP), where the dependence of the complex dielectric permittivity on frequency is here represented in terms of a Cole-Cole function, contrarily to the generally used simple Debye relaxation. The calculated activation energy associated to the conductivity shows a dependence on the anion and is around 65–84 $kJ \cdot mol^{-1}$, which suggests that the ionic conductivity mainly occurs through the vehicle-type mechanism. The diffusivity values follow the trend $D_{NTf2} > D_{Cl} > D_{BF4} > D_{SCN}$, with an associated activation energy (in $kJ \cdot mol^{-1}$) following the trend $E_{act(NTf2)} = 10.9 < E_{act(Cl)} = 12.6 < E_{act(BF4)} = 18.5 < E_{act(SCN)} = 25.1$. The comparison between these values reveals a decrease in the ion binding energies (E_b) and stabilization energies (E_s) could be responsible for the growth of the diffusion coefficient around one or two orders of magnitude depending on temperature and anion. The low stabilization energy observed for the NTF_2^- and Cl^- anions in comparison with NCS^- and BF_4, can be attributed to the poor stabilization of

separated ion pairs by coordination with the PBI segments, which is reflected in the values of the dielectric permittivity (ε_s) calculated by EIS.

INTRODUCTION

The global concern about increasing CO_2 concentration in the atmosphere along the past decade has motivated the scientific community efforts to develop alternative and sustainable energy conversion devices, and has motivated the study of fuel cells (FC), which are electrochemical devices that convert chemical energy into electrical energy in an efficient and clean way.[1] Among the different fuel cell types, proton exchange membrane fuel cells (PEMFC), which use an ion exchange polymer film as the electrolyte, have received increasing attention due to their low operating temperature and quick start–up.[2,3] In this regard, the design of polymer electrolyte materials with high chemical, thermal and mechanical stability combined with elevated conductivity, has absorbed the market in the last decades.[4,5,6] In the commercial scenario of energy applications, several polymeric families have been developed in order to replace the widely used perfluorinated polymers.[7,8] Among these novel polymeric materials, polybenzymidazole (PBI) derivatives have emerged as potential candidates due to their higher thermal and mechanical stability.[9] The most widely used strategy to increase proton conductivity in PBI–based membranes is acid doping, in particular, the use of phosphoric acid (PA) has been stablished as a standard approach, despite its main drawbacks, such as acid leaching and membrane degradation. Along the past decades, different alternatives to PA have been assayed in order to improve the physicochemical properties and performance of PBI membranes such as, inorganic fillers,[10,11] metallic salts,[12,13] carbon-based materials,[14,15] zeolitic imidazolate frameworks (ZIFs),[16,17,18] and ionic liquids (ILs)[19,20,21] among others.

Ionic liquids (ILs) are molten organic salts in which the ions, generally an organic cation with an organic or inorganic anion, are poorly coordinated and consequently, they possess melting points lower than 100 ºC, or are liquids at room temperature.[22,23] Since its discovery, they have been widely used in modern organic chemistry as environmentally friendly solvents in synthesis,[24,25] extraction processes,[26] transport processes,[27] catalysis,[28,29] electrochemistry,[30,31,32] and more recently, as electrically conducting liquids (electrolytes) in the preparation of energy storage and conversion materials.[33] In particular, their low vapor pressure and high chemical stability, in combination with their high ionic conductivity, as they contain mobile ions, have boosted their use as fillers in the preparation of mixed matrix membranes for energy applications.[34] The incorporation of ionic liquids is highly interesting as it allows an efficient transference of the intrinsic properties of the ILs to the polymeric matrix, achieving higher conductivity values at moderate and high temperatures (above 120 ºC), under anhydrous conditions and more importantly, in the absence of mineral acid.[35,36,37] However, scientific efforts have only been focused on the macroscopic properties of the PEM regardless of the analysis of the transport mechanism of the ions inside the polymer matrix, and parameters such as diffusivity and free-charge density are generally omitted. In this way, the study of proton conductivity processes has received intensive attention in the past decades due to their potential applications in fields such as electrochemical devices and fuel cells. Despite the high number of composite membranes which have been described for this purpose, fundamental studies of the conduction phenomena in polymeric membranes with the aim of determining diffusivity and free−charge density and are commonly based on impedance spectroscopy measurements[38] using the electrode polarization (EP) analysis are scarce.

Some of them, which are based on different models proposed by MacDonald–Trukhan,[39,40,41,42] Coelho,[43,44] Schüt,[45,46] Sorensen–Compañ,[47] and Fragiadakis,[48,] among others,[49] are based on the frequency dependence of the complex dielectric loss (ε"), and loss tangent (tan δ) in order to determine the diffusivity and the mobile ion charge density.[50] Generally, the typical analysis of the spectra consists on the separation of polymer relaxation at the high frequency region, the determination of the conductivity in the interval of mid–frequencies and the evaluation of the electrode polarization effect in the low–frequency region, where the real part of the complex permittivity increases considerably.[12] However, in many reported studies, the electrolytes are present in high concentrations and thus, a strong decoupling of the rate of charge transport from the rate of structural polymer relaxation needs to be considered.[51,52,53] Such decoupling has been, in general, solved by correcting the diffusivity using a factor involving the relationship between the mobile charge carrier concentration (determined from the model) and the available ionic charges in the polymer matrix (obtained from experimental ionic concentration).[54,55,56] Consequently, the results obtained by using this correction are more realistic; however, such determination needs to be carried out carefully as it lacks of a justification from a solid theory.

Herein, we describe the synthesis and characterization of different conducting PBI composite membranes containing 1–butyl–3–methylimidazolium (BMIM) with different anionic units ($[Cl]^-$, $[NCS]^-$, $[NTf_2]^-$ and $[BF_4]^-$). The obtained films with different anions were analyzed by electrochemical impedance spectroscopy (EIS) in order to study the influence of the anion on the electrical conductivity, mobility and charge carrier density at temperatures in the range between 20 and 160 ºC. In order to get more insights on the conductivity phenomena, a method based on Coelho model was applied and parameters as diffusivity, mobility and charge carriers density, have been determined using the

electrode polarization method. Within this methodology, the dependence of the complex dielectric permittivity on frequency is represented in terms of a Cole–Cole function instead of the generally applied Debye relaxation.

EXPERIMENTAL SECTION

Materials.

Polybenzimidazole (PBI) with a purity > 99.95% and a molecular weight of 51000 was purchased from Danish Power Systems. 1-Butyl-3-methylimidazolium chloride (BMIM–Cl), 1-butyl-3-methylimidazolium tetrafluoroborate (BMIM–BF_4), 1-butyl-3-methylimidazolium bis(trifluoromethylsulfonyl)imide (BMIM–NTf_2), 1-butyl-3-methylimidazolium thiocyanate (BMIM–NCS), LiCl and N,N–dimethylacetamide (DMAc, 99.8%) were purchased from Sigma-Aldrich and were used without any further purification.

Electrochemical impedance measurements

A Novocontrol broadband dielectric spectrometer concept 80 (Novocontrol Technologies, Hundsangen, Germany) integrated with an SR 830 lock-in amplifier with an Alpha dielectric interface was used to obtain the proton conductivity measurements of the membranes in the transversal direction. The membranes were placed between two gold electrodes coupled to the spectrometer. Initially, the temperature was gradually raised from 20 to 120 °C in steps of 20 °C and the dielectric spectra were collected at each step. A second cycle of temperature scan (named as anhydrous conditions in the manuscript), the dielectric spectra were collected at each step from 0 to 200 °C in steps of 20 °C. The frequency interval was from 10^{-1} to 10^{7} Hz, applying a 0.1 V signal

amplitude. The membranes were previously immersed in deionized water and the thickness was measured afterwards using a digital micrometer, taking the average measurements at different parts of the surface.

RESULTS AND DISCUSION

Preparation and characterization of PBI membranes containing ionic liquids.

Composite PBI membranes containing 5 wt. % of ionic liquid were prepared by conventional casting method. To this end, the ionic liquid (0.05 g) was dissolved in a 10 wt. % PBI solution in DMAc (10 g) under vigorous stirring to give a final PBI solution with 5 wt. % of ionic liquid. The ionic liquid concentration in the PBI solution was in the range of 0.04 M. This solution was cast onto a clean glass petri dish and heated at 80 °C for 8 h, followed by a subsequent drying at 160 °C for 10 h in order to remove the organic solvent. Next, membranes were carefully peeled of the petri dish and dried under pressure at 150 °C for 10 min. A washing by immersion in distilled water at 80 °C was performed in order to remove residual solvent (DMAc) from the membrane, followed by a final drying at 160 °C for 16 h. After all these steps, transparent membranes with an average thickness of 100 μm were obtained. All composite membranes containing 5 wt. % of IL displayed water uptake and swelling ratios higher than those observed for pristine PBI membrane (Table S1in the Supporting Information).

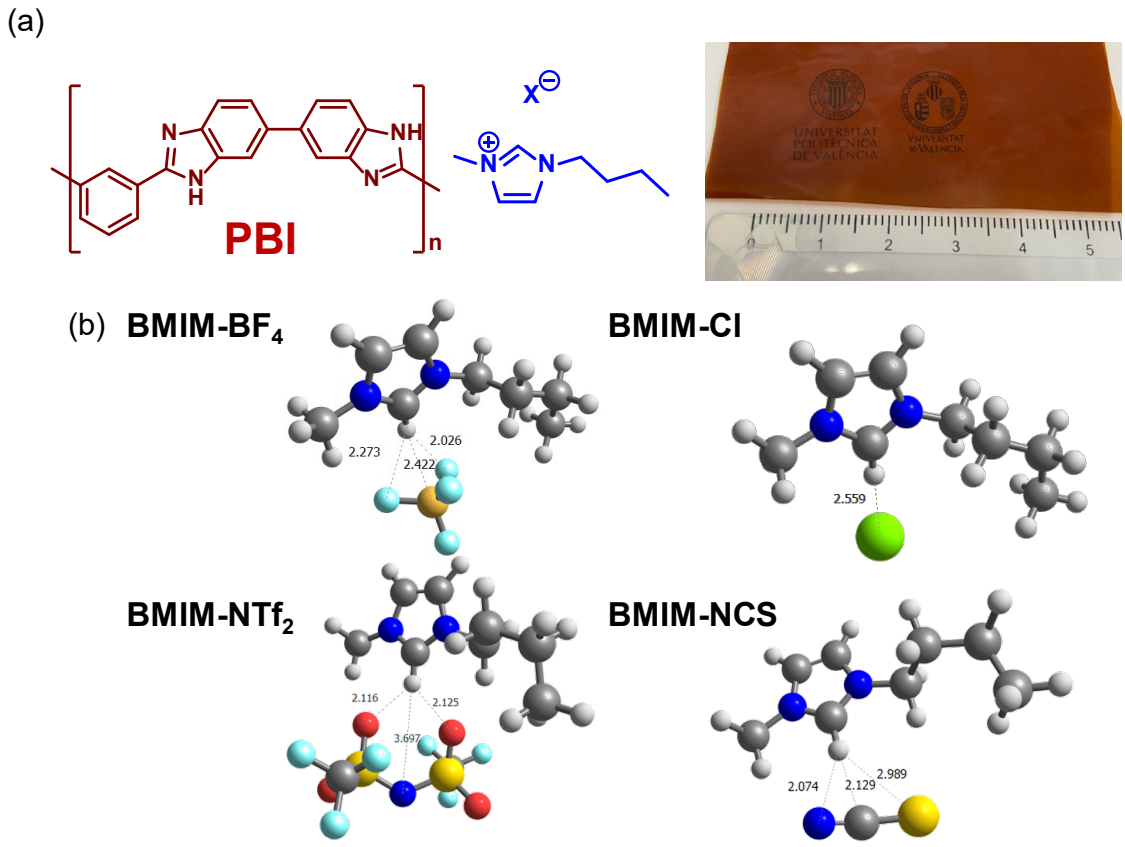

Figure 1. (a) Chemical structure of PBI and BMIM-derived ionic liquid. Photograph of PBI composite membrane PBI@BMIM–NTf_2 containing 5 wt. % of BMIM–NTf_2. (b) Optimized structures for BMIM and different anions used in this study.

All prepared membranes were fully characterized by attenuated total reflection Fourier transform infrared (ATR–FTIR) spectroscopy, thermogravimetric analysis (TGA), oxidative stability by immersion in Fenton's reagent and mechanical behavior as previously described.[57] Briefly, no significant changes in morphology were observed even after analyzing the cross section SEM images of composite membranes (**see Figure S1, Supporting Information**). Infrared spectroscopy study revealed the incorporation of the IL into the polymeric matrix, as shown in Figure 2a. All FT–IR spectra of the 5 wt. % IL–PBI composite membranes showed typical bands of PBI, such as a broad peak around 3500–3200 cm^{-1} (ν_{N-H} stretching) and bands at 1607 and 1421 cm^{-1}, which are associated with $\nu_{C=N}$ and ν_{C-N} stretching, respectively [46]. The incorporation of BMM–NTf_2 in the

was confirmed by the presence of peaks associated to the bis(trifluoromethylsulfonyl)imide anion at 1192 cm^{-1} (ν_{CF3} stretching), 1131 cm^{-1} (ν_{SO2} symmetric stretching) and 1052 cm^{-1} (ν_{S-N} stretching) [47]. For PBI@BMIM–NCS membrane, a characteristic band from the thiocyanate group was observed at 2060 cm^{-1}. Thermogravimetric analysis (TGA) of the membranes showed these materials are stable up to 300 °C, showing that composite membranes possessed enough thermal stability for its application in high temperature PEMFCs, which operate at temperatures above 140 °C (Figure 2b). The mechanical (Figure 2c and Table S2in the Supporting Information) and chemical stability (evaluated with Fenton's test, Figure 2d)[58] of the IL–containing PBI membranes was superior to that of the pure PBI membrane. Consequently, it can be concluded that all the composite membranes containing ILs showed an excellent mechanical and thermal stability, while being flexible and transparent.

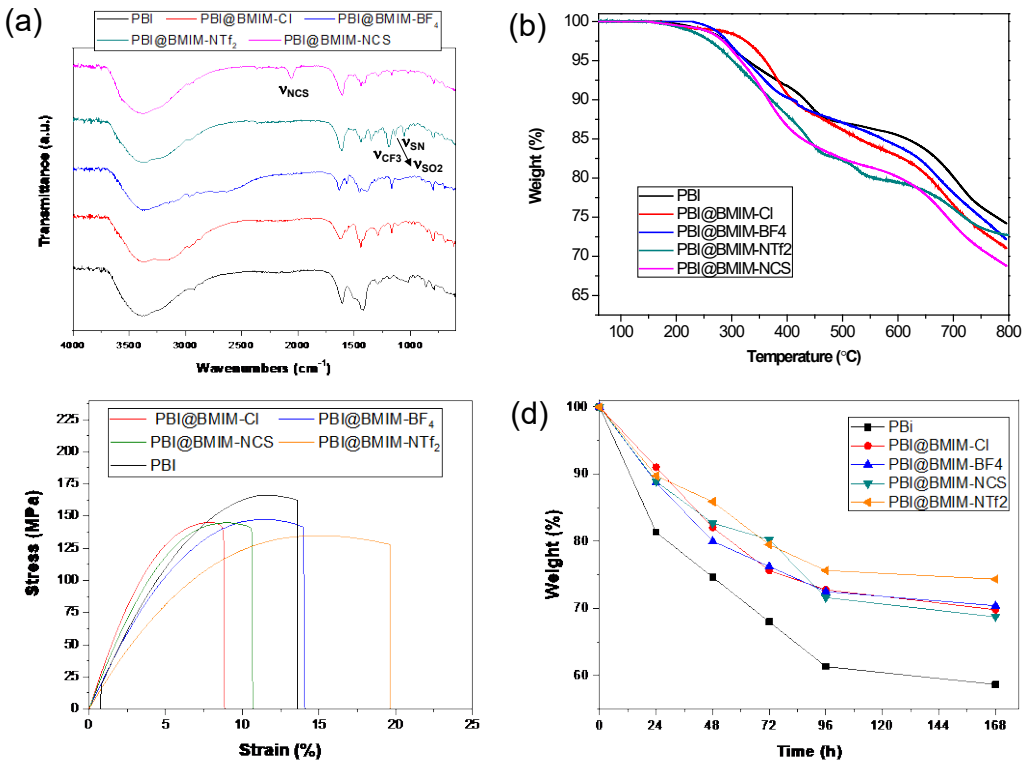

Figure 2. (a) TGA curves under a N_2 atmosphere, (b) stress-strain curves and (c) Fenton's test of PBI composite membranes containing 5 wt. % of different ionic liquids derived from BMIM.

Dielectric properties

The ionic conductivity of the PBI composite membranes containing ILs was measured in the transversal direction by electrochemical impedance spectroscopy (EIS) along the temperature range of 20–160 ºC in the frequency range from 10^{-1} to 10^{7} Hz, applying a 0.1 V signal amplitude. From the complex dielectric measurements, the complex conductivity is given by $\sigma^*(\omega,T) = j \cdot \varepsilon_0 \cdot \omega \cdot \varepsilon^*(\omega,T)$, which can be expressed in terms of the real and imaginary part taking into account the dielectric permittivity $\varepsilon^*(\omega) = \varepsilon'(\omega) + j\varepsilon''(\omega)$, where ε_0 represents the vacuum permittivity, ω is the angular frequency of the applied electric field ($\omega = 2\pi f$) and j is the imaginary unity ($j^2 = -1$).

In polyelectrolytes such as polymers and electrolytic membranes, the real part of conductivity, namely σ' (i.e. σ_{dc}), can be obtained from the Nyquist diagrams, where the complex conductivity (σ") is plotted against the real part of the conductivity (σ'). These representations display a typical semicircle with a spike at high frequencies, as shown in Figure 3, except for PBI membrane containing thiocyanate as counterion, which showed a different behavior.

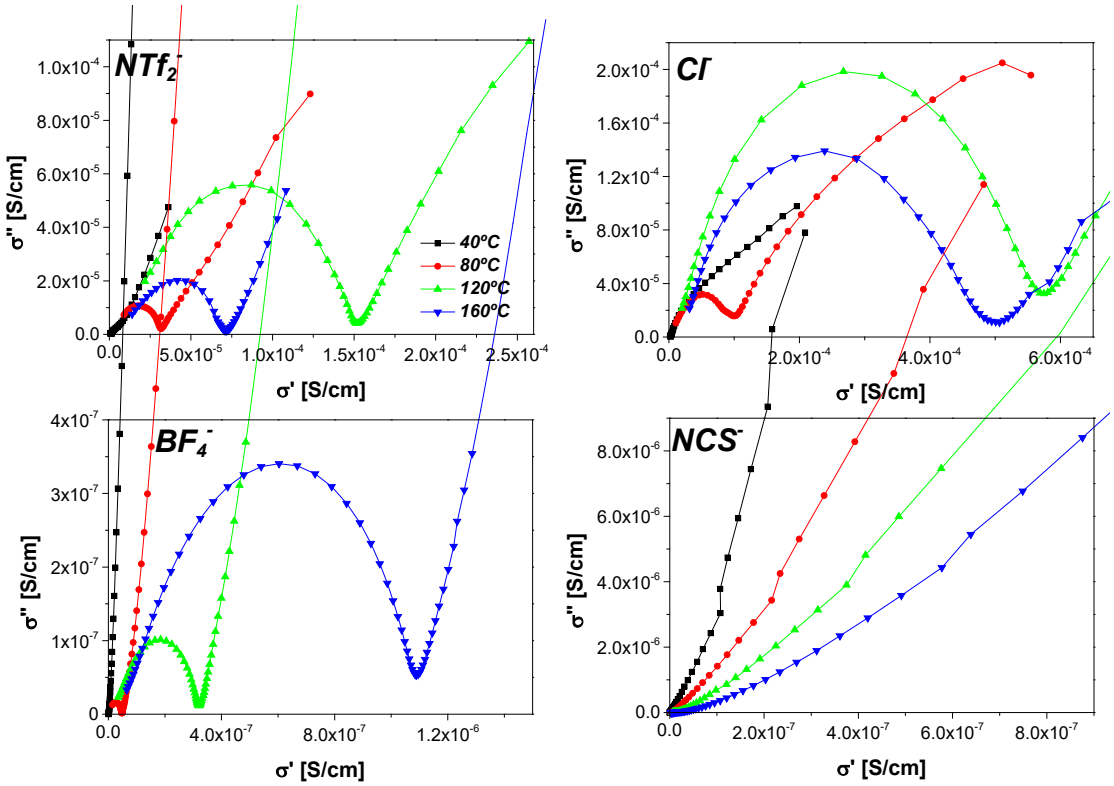

Figure 3. Nyquist plots of the complex conductivity spectra of the PBI composite membranes containing BMIM with different anions at 40, 80, 120 and 160 °C.

As shown in Figure 3, which shows a representation of the imaginary part of the conductivity (σ" (S/cm) vs. the real part of the conductivity (σ' in (S/cm), all composite membranes except PBI@BMIM-NCS displayed Nyquist plots with semicircles intersecting the abscissa axis at $\sigma' = \sigma_{dc}$. At the intersection point with the abscissa axis, the imaginary part of the complex conductivity is equal to zero (i.e., the phase angle is zero) and then, this value represents the dc–conductivity of the membrane,[59] which is related with its resistance, R_0, by the expression:

$$\sigma' = \sigma_{dc} = \frac{L}{S}\frac{Z'}{\left[(Z')^2 + (Z'')^2\right]} = \frac{L}{S \cdot R_0} \qquad (1)$$

where L is the thickness of the sample, S the effective area of the membrane (given by the area of the electrodes used for the measurement), and Z' and Z" are the real and

imaginary part of the complex impedance, respectively. As inferred from Figure 3, the intercept of semicircles in the x–axes increases with temperature, as typically observed for composite membranes. As shown, for PBI@BMIM–Cl, PBI@BMIM–NTf2 and PBI@BMIM–BF_4 membranes, a spike can be observed in experimental Nyquist diagrams at temperatures above 40 ºC (Figure 3). It is worth mentioning that the semicircles are not present in measurements below 40 ºC because it should be present at frequencies higher than 10 MHz. Departure from semicircles can be observed in experimental Nyquist diagrams because of polarization processes and other phenomena, which might be taking place in the sample/electrode interface. As consequence, the distribution of the relaxation time causes the depression in the semicircles. In the case of PBI@BMIM–NCS, the semicircle curve vanished leaving only the tilted spike, which can be explained by the increasing of the resistance of this membrane indicating that conductivity will be mainly due to the hopping of NCS- ions.

Typically, these results are interpreted in terms of equivalent circuits formed by a resistance R_0 in series with a circuit composed of a resistance R_p, representing the charge transfer resistance at the interface sample/electrode, connected in parallel with a constant phase element (CPE), which is equivalent to the sample/electrode double layer (**Figure S2, Supporting Information**).

Accordingly, the values of dc–conductivity for all composite membranes at different temperatures were calculated and displayed in Figure 4 (Similar values have been observed from the Bode diagrams shown in Figure S3, Supporting Information). As shown, the conductivity for PBI@BMIM–Cl and PBI@BMIM–NTf_2 membranes increased with temperature until reaching a maximum value at 140 ºC, and then, a droped in conductivity was observed at higher temperatures. On the other hand, for

PBI@BMIM–NCS and PBI@BMIM–BF_4 membranes, the conductivity increased with temperature in all the range of temperatures under study; however, the values were lower in comparison with those of PBI@BMIM–Cl and PBI@BMIM–NTf_2. The enhancement of conductivity in these membranes can be explained by the effects of the physicochemical properties of the plasticizer, which possesses a higher relative dielectric permittivity (usually denoted as the static dielectric constant) in the absence of electrode polarization ($\varepsilon_S=\varepsilon_\infty$), 35 and 50 in our study for PBI@BMIM–Cl and PBI@BMIM–NTf_2, respectively. The higher value of ε_∞ can decrease pair interaction energy (E_d), by weakening the Coulombic force that exists between the anions (NTf_2^- and Cl^-) and the cation (BMIM), increasing the concentration of mobile anions in the membrane, and consequently, increasing the ionic conductivity. On the other hand, for PBI@BMIM–NCS and PBI@BMIM–BF_4 membranes, dielectric constant were 10-fold lower (3.5 and 4.5, respectively). This phenomena has been also reported in other studies where the effective dissociation energy determined from the measured interaction decay length was in agreement with the calculation of the ion pair energy using a simple model.[60,61] Similarly, if the dielectric permittivity of the membrane increases, the Debye length would also increase, as previously discussed.

Such behavior can be attributed to the mobility of the anion from of the IL and the carrier charge density of the IL incorporated to the polymer matrix of the PBI. In this regard, the mobility of the anion can be interpreted in terms of the interaction energy of the anion and the cation (BMIM) In order to evaluate the anion mobility, interaction energies were calculated by means of quantum mechanics calculations using the widely used B3LYP functional[62] and the 6–311+G(d,p) basis set as implemented in Gaussian 16.[63] The computed energies show values around 300 $kJ \cdot mol^{-1}$ for BMIM–NCS and BMIM–BF_4, in contrast with the 265 and 272 $kJ \cdot mol^{-1}$ for BMIM–NTf_2 and BMIM–Cl,

respectively. These values suggest that membranes containing $[NTf_2]^-$ and $[Cl]^-$ may have a better anion mobility and consequently higher through plane conductivity. In this regard, conductivities up to 0.001 $S \cdot cm^{-1}$ were reached at 140 ºC for the PBI@BMIM–Cl, being similar to other previously described PBI composite membranes.[11] However, it is not easy to stablish a fair comparison as most reported examples use phosphoric acid as doping agent and under these conditions, conductivities up to 0.1 $S \cdot cm^{-1}$ can be generally reached. Despite the high conductivity of these PA-doped membranes, studies on acid leaching and membrane degradation are generally omitted.

In general, the conductivity behavior with temperature follows the Arrhenius equation given by the expression $\ln \sigma_{dc} = \ln(\sigma_0) - (E_{act}/RT)$, where σ_{dc} is the proton conductivity of the membrane ($S \cdot cm^{-1}$), σ_0 is a pre-exponential factor ($S \cdot cm^{-1}$), E_{act} is the activation energy ($kJ \cdot mol^{-1}$), R is the ideal gas constant (8.314 $J \cdot mol^{-1} \cdot K^{-1}$) and T is the temperature (K). From the ln (σ_{dc}) vs. (1000/T) plot, the activation energy of a given sample can be obtained from the slope of the linear fit.

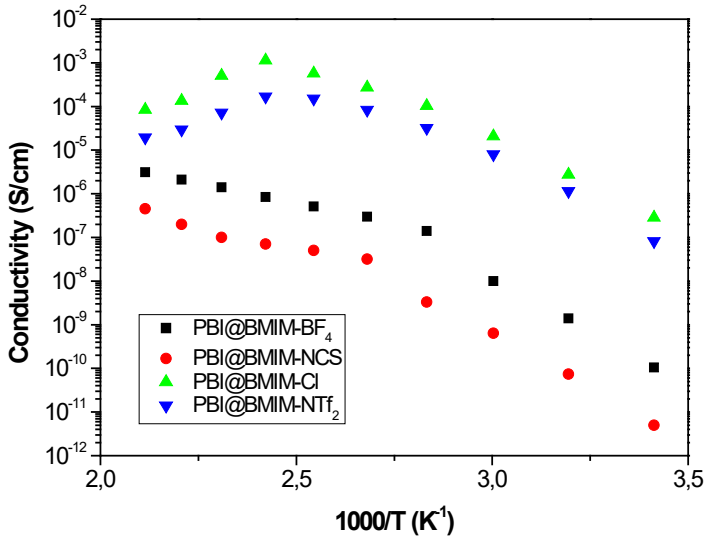

Figure 4. Variation of the conductivity versus 1000/T for PBI composite membranes.

The activation energy associated to the conductivity is dependent of anion type and follows the trend $E_{act}(NTF_2^-) < E_{act}(Cl^-) < E_{act}(BF_4^-) < E_{act}(NCS^-)$. The estimated values for the activation energies of these membranes are in the range of 65–84 $kJ \cdot mol^{-1}$, which suggests that the ionic conduction in these compounds mainly occurs through the vehicle-type mechanism. However, a close inspection reveals a change in the slopes. For PBI@BMIM–NTf_2 and PBI@BMIM–Cl, a negative slope is present at high temperatures, in contrast with a slightly positive for PBI@BMIM–NCS and PBI@BMIM–BF_4. This behavior can be associated to the variation in Debye's length, which is related with the effective dissociation energy and the measured dielectric permittivity in absence of electrode polarization (ε_∞), as well as of orientational polarization of dipolar ions, as previously reported.[64,65]

The obtained values follow a similar trend that the computed association energies obtained by DFT calculations. These values show that PBI@BMIM–NTF_2 and PBI@BMIM–Cl, which have lower activation energies, are more attractive to be applied as polymer electrolyte membranes in energy applications, as the transport mechanism is less energy demanding.

Diffusivity and free-charge density

Typically, the dependence of the complex dielectric permittivity on frequency is represented by a single Debye relaxation;[44] however in this work, we have expressed it following a different model based on a Cole–Cole function by means of the expression:

$$\varepsilon_{EP}^{*} = \varepsilon_{\infty} + \frac{\Delta\varepsilon_{EP}}{1 + (j\omega\tau_{EP})^{\alpha}} \tag{2}$$

where $\Delta\varepsilon_{EP} = \varepsilon_{EP} - \varepsilon_{\infty}$, being ε_{EP} the dielectric constant when the EP is completely buildup, and ε_{∞} the static dielectric constant of the sample. The term τ_{EP} is the macroscopic relaxation time of EP, and is the time required for an ion to travel from one electrode to the other through the sample. Finally, the α exponent is the indication of cumulative process in the system as consequence of the interactions among charge carriers and j the imaginary unity. The main difference between the Cole–Cole and Debye descriptions is essentially, the α exponent, which describes sub-diffusion when $\alpha < 1$. This exponent is the manifestation of cumulative processes in the system that are related to interactions among charge carriers. When $\alpha \ll 1$ these interactions are strong, and in contrast, when $\alpha \lesssim 1$ the interactions do not dominate the transport process. Therefore, it is expected that high conductivity processes will be associated to $\alpha \lesssim 1$.

Firstly, assuming that the contribution of the conductivity at low frequencies can be omitted, which is generally due to impurities, and secondly, the expressing the dc–conductivity from the imaginary part of the permittivity, when the Maxwell–Wagner–Sillars (MWS) conditions are accomplished,[66,67] (i.e., when the bulk conductivity dominates as for a pure ohmic conduction at high frequencies), then $\varepsilon''(\omega,T) = \sigma_{dc}(\omega,T)/\varepsilon_0\omega$, the loss tangent, $\tan = \varepsilon'' / \varepsilon'$, can be expressed as follows:

$$\tan\delta = \frac{\Delta\varepsilon_{EP}(\omega\tau_{EP})^{\alpha}\sin\left(\frac{\pi\alpha}{2}\right) + \frac{\sigma_{dc}}{\varepsilon_0\omega}\left[1 + 2(\omega\tau_{EP})^{\alpha}\cos\left(\frac{\pi\alpha}{2}\right) + (\omega\tau_{EP})^{2\alpha}\right]}{\varepsilon_{\infty}\left[1 + 2(\omega\tau_{EP})^{\alpha}\cos\left(\frac{\pi\alpha}{2}\right) + (\omega\tau_{EP})^{2\alpha}\right] + \Delta\varepsilon_{EP}\left[1 + (\omega\tau_{EP})^{\alpha}\cos\left(\frac{\pi\alpha}{2}\right)\right]} \quad (3)$$

Following the consideration by Klein *et al.*,[68] when dc-conductivity is lower than 10^{-5} S·cm^{-1} and τ_{EP}>1 s, the term with σ_{dc} in Equation 3 has a negligible effect on the expression of *tan* δ, and therefore also in the *tan* δ peak. However, for conductivities higher than 10^{-5} S·cm^{-1}, the maximum peak in loss tangent can be markedly affected by

the conductivity. In our case, this term can affect significantly in case of PBI@BMIM-Cl and PBI@BMIM-NTf_2 membranes. Under these conditions, Equation 3 can then be simplified to:

$$\tan\delta = \frac{(\omega\tau_{EP})^{\alpha}\sin\left(\frac{\pi\alpha}{2}\right) + \frac{\sigma_{dc}}{\varepsilon_0\Delta\varepsilon_{EP}\omega}\left[1+2(\omega\tau_{EP})^{\alpha}\cos\left(\frac{\pi\alpha}{2}\right)+(\omega\tau_{EP})^{2\alpha}\right]}{1+2(\omega\tau_{EP})^{\alpha}\cos\left(\frac{\pi\alpha}{2}\right)+\frac{(\omega\tau_{EP})^{2\alpha}}{M}} \quad (4),$$

with $M=\Delta\varepsilon_{EP}/\varepsilon_{\infty}$. Notice that if $\alpha=1$ and ionic conductivity is lower than 10^{-5} $S\cdot cm^{-1}$, then Equation 4 is reduced to Coelho model, where EP behavior is represented by a single Debye relaxation.

Figure 5 shows the tan δ as a function of the frequency for all the samples studied at different temperatures. As shown, a maximum in the curves at each temperature is observed, which is associated to the plateau of the real part of the conductivity observed in the Bode diagrams (**see Fig. S3 in the Supporting Information**).

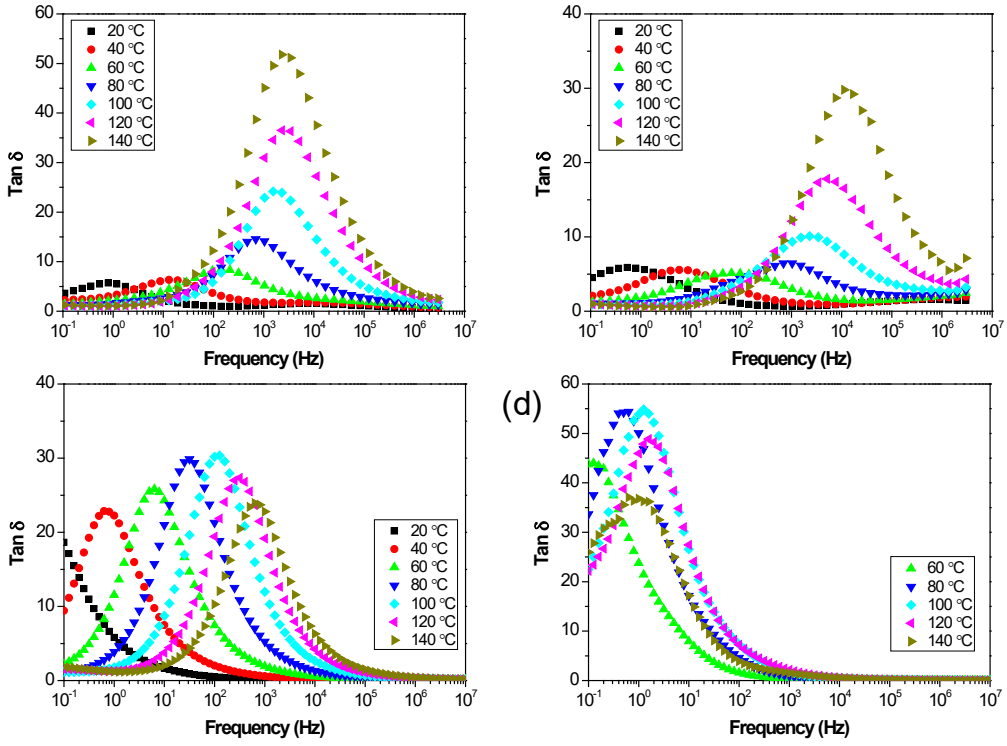

Figure 5. Tan δ vs. frequency for (a) PBI@BMIM−NTf_2, (b) PBI@BMIM−Cl, (c) PBI@BMIM−BF_4 and (d) PBI@BMIM−NCS at different temperatures.

From electrochemical impedance spectroscopy measurements, the loss tangent for each one of the membranes was obtained in the range of temperatures between 20 and 160 °C. From Figure 5 we a clearly maximum in the curves at each temperature was observed, and a shifting to high frequencies a function of temperature. However, the behavior is different depending on the anion. For example, for the $[NTf_2]^-$ and $[Cl]^-$ the increase in the temperature produces a growth in maximum intensity. However, for $[BF_4]^-$ and $[SCN]^-$, the intensity decreases when the temperature increases until 100 ºC, and then gradually rises with temperature.

Table 1. Calculated values for M, τ_{EP} and α using Equation 4 for the range of temperatures between 20 and 160 ºC.

	T = 20°C			**T = 40°C**		
Membrane	**M**	**τ_{EP} (s)**	**α**	**M**	**τ_{EP} (s)**	**α**
PBI@BMIM-NTf2	$(7.62\pm0.15)\times10^{2}$	$(9.44\pm0.19)\times10$	0.883±0.018	$(1.26\pm0.03)\times10^{3}$	$(6.92\pm0.14)\times10^{-1}$	0.885±0.018
PBI@BMIM-Cl	$(4.16\pm0.08)\times10^{3}$	$(4.27\pm0.09)\times10$	0.845±0.017	$(2.50\pm0.5)\times10^{3}$	(2.94±0.06)	0.848±0.017
PBI@BMIM-BF4	-	-	-	$(9.52\pm0.19)\times10^{3}$	$(2.38\pm0.05)\times10$	0.978±0.020
PBI@BMIM-SCN	-	-	-	-	-	-
	T = 60°C			**T = 80°C**		
Membrane	**M**	**τ_{EP} (s)**	**α**	**M**	**τ_{EP} (s)**	**α**
PBI@BMIM-NTf2	$(3.14\pm0.06)\times10^{3}$	$(9.71\pm0.19)\times10^{-2}$	0.903±0.018	$(8.73\pm0.18)\times10^{3}$	$(2.64\pm0.05)\times10^{-2}$	0.941±0.019
PBI@BMIM-Cl	$(4.21\pm0.08)\times10^{3}$	$(4.43\pm0.09)\times10^{-1}$	0.825±0.017	$(6.46\pm0.13)\times10^{3}$	$(4.87\pm0.10)\times10^{-2}$	0.847±0.017
PBI@BMIM-BF4	$(1.130\pm0.023)\times10^{4}$	(2.97±0.06)	0.975±0.020	$(1.53\pm0.03)\times10^{4}$	$(6.77\pm0.14)\times10^{-1}$	0.977±0.020
PBI@BMIM-SCN				$(1.20\pm0.02)\times10^{5}$	$(1.16\pm0.02)\times10^{2}$	0.984±0.020
	T = 100°C			**T = 120°C**		
Membrane	**M**	**τ_{EP} (s)**	**α**	**M**	**τ_{EP} (s)**	**α**
PBI@BMIM-NTf2	$(2.04\pm0.04)\times10^{4}$	$(1.40\pm0.03)\times10^{-2}$	0.966±0.019	$(6.86\pm0.14)\times10^{4}$	$(1.58\pm0.03)\times10^{-1}$	0.975±0.020
PBI@BMIM-Cl	$(8.99\pm0.02)\times10^{4}$	$(1.21\pm0.24)\times10^{-2}$	0.907±0.018	$(1.68\pm0.03)\times10^{4}$	$(5.13\pm0.10)\times10^{-3}$	0.951±0.019
PBI@BMIM-BF4	$(1.54\pm0.03)\times10^{4}$	$(1.86\pm0.40)\times10^{-1}$	0.979±0.020	$(1.12\pm0.02)\times10^{4}$	$(6.08\pm0.12)\times10^{-2}$	0.978±0.020
PBI@BMIM-SCN	$(1.14\pm0.02)\times10^{5}$	$(4.66\pm0.09)\times10^{1}$	0.984±0.020	$(8.83\pm0.18)\times10^{4}$	$(3.32\pm0.07)\times10^{1}$	0.982±0.020
	T = 140°C			**T = 160°C**		
Membrane	**M**	**τ_{EP} (s)**	**α**	**M**	**τ_{EP} (s)**	**α**
PBI@BMIM-NTf2	$(9.62\pm0.19)\times10^{4}$	$(1.85\pm0.04)\times10^{-1}$	0.980±0.020	$(1.67\pm0.03)\times10^{5}$	$(3.38\pm0.07)\times10^{-2}$	0.982±0.020
PBI@BMIM-Cl	$(4.41\pm0.09)\times10^{4}$	$(3.12\pm0.06)\times10^{-2}$	0.970±0.019	$(8.25\pm0.17)\times10^{4}$	$(2.71\pm0.05)\times10^{-3}$	0.980±0.020
PBI@BMIM-BF4	$(8.66\pm0.17)\times10^{3}$	$(2.52\pm0.05)\times10^{-2}$	0.975±0.020	$(7.35\pm0.15)\times10^{3}$	$(1.23\pm0.03)\times10^{-2}$	0.967±0.019
PBI@BMIM-SCN	$(8.96\pm0.18)\times10^{4}$	$(6.50\pm0.13)\times10^{1}$	0.975±0.020	$(2.88\pm0.06)\times10^{4}$	$(6.17\pm0.12)\times10^{1}$	0.937±0.019

On the other hand, the width of relaxation is greater in the case of $[NTf_2]^-$ and $[Cl]^-$ than $[BF_4]^-$ and $[SCN]^-$ ions, and the peaks are observed at lower frequencies than the others are. Equation 4 was used to fit the experimental data shown in Figure 5 to provide the estimation for M, τ_{EP} and α. The values of these parameters are given in Table 1, for the temperatures compress in the range of temperatures between 20 and 160 ºC, respectively. The standard deviation of M, τ_{EP} and α parameters determined from the fitting curves remaining less than 5%. It is worth mentioning that he calculated values for the parameter α are below 1, meaning that interactions are present but they are not dominant on the transport process. It is also observed that the relaxation time τ_{EP} and the parameter M, showed a dependence on the temperature. A close inspection of this the value reveals that M increase with the temperature increase for all the membranes, and τ_{EP} decrease with the temperature increase, but it is higher for the PBI@BMIM–NCS membrane. In Figure 6, it can be seen the fitting for the four membranes under study at four different temperatures (40, 80, 120 and 160 ºC), where a good agreement between the fit, using Eq.(4), with experimental data is It is clearly stated.

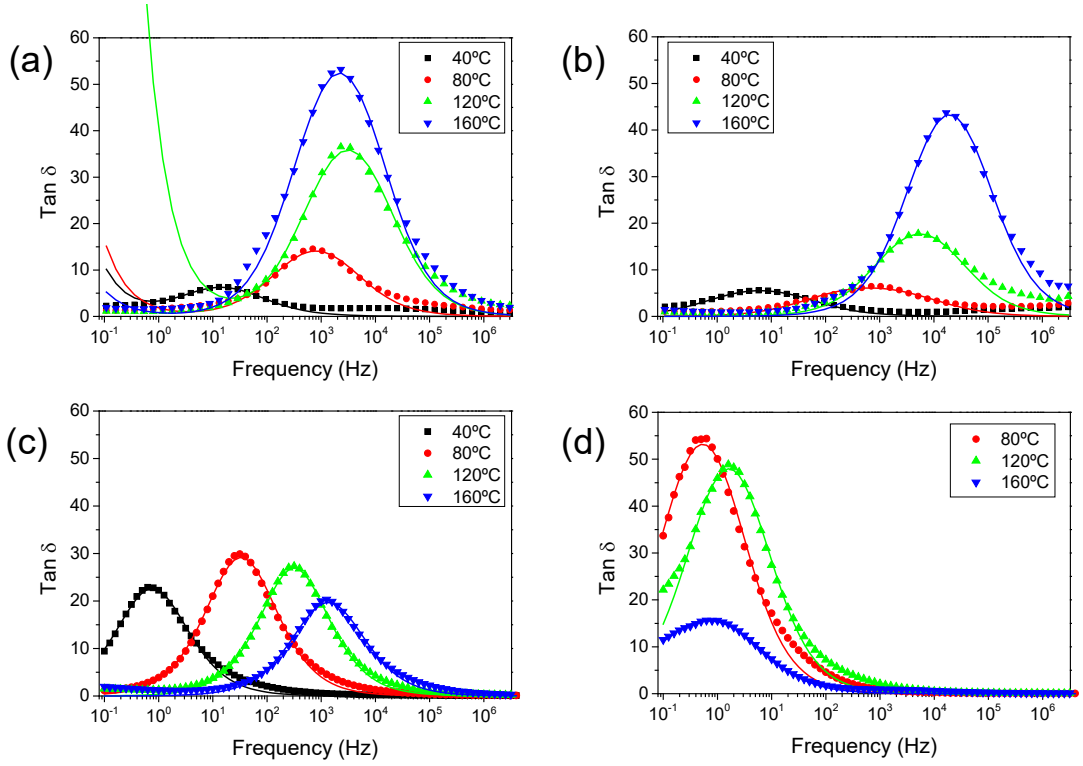

Figure 6. Fitting for tan δ vs frequency at different temperatures for (a) PBI@BMIM–NTf_2, (b) PBI@BMIM–Cl, (c) PBI@BMIM–BF_4 and (d) PBI@BMIM–SCN.

The curves shown in Figure 6, display peaks corresponding to the maxima in tan δ (Eq. (5)) and are associated with the intersect of the semicircles in σ'-σ" Cole-Cole plot with the real axis which value represent the dc-conductivity. Similarly, the peaks observed in tan δ are also associated with the plateau showed in Bode diagram plotted in figure S3 (Supplementary Information). Their corresponding values in frequency are related with the parameters *M,* τ_{EP} and α as

$$\tau_{EP}(\alpha) = \frac{M^{\frac{1}{2\alpha}}}{\omega_{max}^{tan\delta}} = \tau_m M^{\frac{1}{2\alpha}} \qquad (5)$$

where $\omega_{max}^{tan\delta} = 1/\tau_m$ is the reciprocal of the relaxation time corresponding to the frequency where tan δ shows a maximum. This relaxation time is associated to the ionic conduction mechanism in the membrane.

Assuming that $L = (D\tau_{EP})^{1/2}$, the effective diffusivity (D) of mobile carriers through the samples can be estimated. In general the measured conductivity is a sum of the contributions of all the constituent charge carriers, i.e. $\sigma_{dc} = \sigma^{+}+\sigma^{-}$, considering that both cations and anions have the same valence. Assuming that all the available ions take part in charge transport, the highest possible contribution of the anions to the total conductivity can be estimated supposing that anion transference number is practically equal to one. In this approximation, the cations are practically immobile due to the reduced mobility that BMIM cation as a consequence of its size in comparison with the other counterpart. Therefore, the cation mobility is negligible and then, the dominated mobility will be mainly restrictive to the anion contribution. Then, the effective diffusivity can be calculated using Equation 5 as

$$\boldsymbol{D = \frac{L^2}{4\tau_m M^{3/2\alpha}}} \qquad (6)$$

where, the parameters τ_m, M and α can be obtained using the Equation 4, and by fitting the loss tangent curves .

It is worth mentioning that Equation 6 is the same than that determined using the Klein model,[69] but changing τ_m by τ_{EP} and considering the eq.(5).

Bandara *et al.*[49] used the relaxation time (τ) as the relaxation time corresponding to the frequency where tan δ shows a maximum, i.e. $\tau = \tau_m$. With this consideration and assuming $L = (D\tau_m)^{1/2}$, an erroneous expression for the diffusion coefficient ($\boldsymbol{D = \frac{L^2}{4\tau_m M^2}}$), was obtained.[49] Notice the clear difference with our Eq.(6) through the exponent.

Next, considering that only one type of ions are freely mobile through the membrane, the anion mobility (μ) can be obtained from the diffusivity, taking into

account that dc-conductivity can be approximately written versus the effective mobility and considering the Nernst-Einstein relation from

$$\sigma_{dc} = nq|Z|\mu = nq^2|Z|^2 \frac{D}{K_B T} \quad (7)$$

Where, q is the charge of anion, Z the valence of the charge, n is the equilibrium number density of free negative charges, k_B is the Boltzmann constant and T the absolute temperature.

Then, the mobility can be calculated from

$$\boldsymbol{\mu} = \frac{q\ \boldsymbol{L^2}}{\boldsymbol{4\tau_m M^{3/2}}\ k_B\ T} \quad (8)$$

Finally, the mobile charge density (n) can be calculated from the dc-conductivity and the mobility as:

$$\boldsymbol{n} = \frac{\boldsymbol{\sigma_{dc}}}{\boldsymbol{q\mu}} = \frac{\boldsymbol{4\sigma_{dc}\tau_m M^{3/2}}\ k_B\ T}{q^2\ \boldsymbol{L^2}} \quad (9)$$

Taking into account the values of the parameters gathered in Table 1, we have calculated the values for diffusivity D using Equation 6, the mobility and charge density n with Equations 8 and 9, respectively. The results obtained for diffusivity and mobility as a function of the temperature are shown in Figures 7 and 8 respectively. The error in the estimation of diffusivity, mobility and charge carriers density from Equations 6-9 correspond to the standard deviation being generally less than 10%. On the other hand, we can see that for the sample PBI@BMIM–NCS only at temperatures higher than 80 ºC the peak in loss tangent were observed and from our model the values of D, μ and n only will be possible calculate for this interval of temperatures.

The values for the diffusion coefficients increase with temperature increases and are reasonably similar to those reported for other related systems. A close inspection of

the variation of the values represented in the activation plot in Figure 7 allows indicates the excellent ion diffusivities that can be obtained with these films. The diffusivity rises as the temperature for all the samples following the trend $D_{NTf2} > D_{Cl} > D_{BF4} > D_{SCN}$. From the VFT fit, we calculated the activation energy associated to the diffusivity, and follow the trend $E_{act(NTf2)} = 10.9 < E_{act(Cl)} = 12.6 < E_{act(BF4)} = 18.5 < E_{act(SCN)} = 25.1$ kJ·mol^{-1}. The comparison between them reveals that a decrease in the ion binding energies (E_b) and stabilization energies (E_s), could be responsible for the growth of the diffusion coefficient around one or two orders of magnitude depending of the temperature and ion type. An estimation of the ion binding energy E_b, and stabilization energy E_s, can be approximately obtained following the same procedure than Klein et al.[69], from $E_{act} = E_b - E_s$, where $E_b = -q^2/(4\pi\varepsilon_0 \varepsilon_\infty r)$, being ε_0 the vacuum permittivity, ε_∞ the dielectric constant of the sample and r the separation between centers of contact ions (2.12 , 2.56 , 2.42 and 2.19 Å, for $[NTf_2]^-$, $[Cl]^-$, $[BF_4]^-$ and $[SCN]^-$, respectively, see Figure 1). The values calculated for E_b and E_s, taken the distances between the centers of the ions pairs, are given in Table 2. The values found for the ion binding energy are larger than experimental activation energy. However, a low stabilization energy was observed for the NTF_2^- and Cl^- anions in comparison with NCS^- and BF_4, which can be attributed to the poor stabilization of separated ion pairs by coordination with the PBI segments, which is reflected in the values of the dielectric permittivity (ε_s), calculated from $E_d = \frac{E_{pair}}{\varepsilon_s}$, insomuch as the value of ε_s is in the range of 4-5 for PBI@BMIN–BF_4 and PBI@BMIN–NCS, while they are one order in magnitude higher for PBI@BMIN–NTf_2 and PBI@BMIN–Cl.[64]

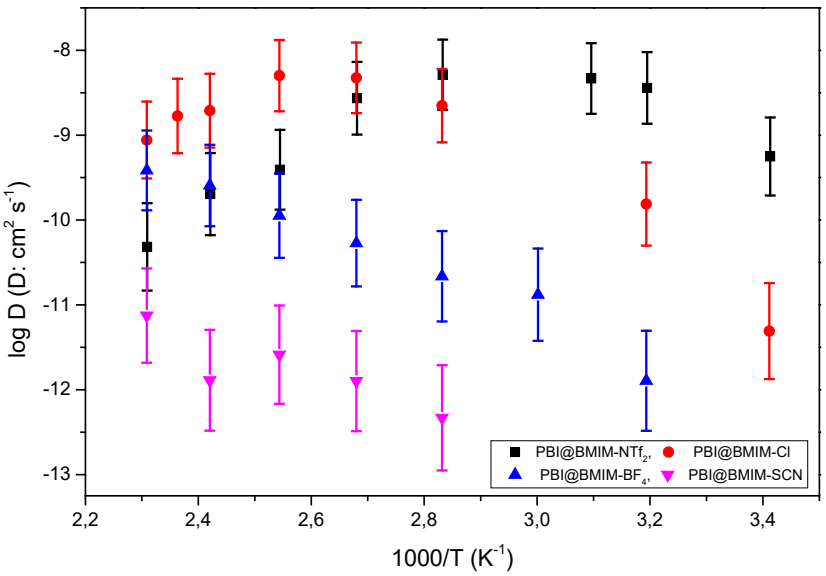

Figure 7. Temperature dependence of diffusivity for the different anions ionic liquids composite PBI membranes.

The ion mobility calculated from electrode polarization model through Eq.(8) is shown in Figure 8. The values obtained are well described using the VFT equation ($\ln \mu = \ln \mu_\infty - B/(T-T_0)$), and the fitting parameters are listed in Table 2. A close inspection of Figure 8 shows that mobility increase with temperature increase and is between two or three orders of magnitude higher when the anion is Cl^- and NTf_2^-, respect the BF_4^- and NCS^- anions, respectively. These results are in agreement with the diffusivities and conductivities observed. It is possible due to the strong electrostatic interaction between ion pairs and mobile anions assuming the formation of transient pairs in the case of BF_4 and NCS anions producing a diminution of carrier charge density into the polymeric matrix for PBI@BMIN–BF_4 and PBI@BMIN–NCS. Another plausible explanation could be related with the effective Debye length values corresponding to this type of composite membranes, in which ionic liquids are present in the bulk of polymeric matrix. Accordingly, we calculated the Debye length (L_D) from the values obtained for the

parameter M ($M = L/(2L_D)$)[69] by the fitting curves of loss tangent vs. frequency. These results show that PBI@BMIN−BF_4 and PBI@BMIN−NCS membranes have a Debye length comprised around 1-2 nm at 100 ºC, while for PBI@BMIN−NTf_2 and PBI@BMIN−Cl Debye lengths are around one hundred times higher (**see Fig. S4 in the Supporting Information**).

Table 2. Activation energy (E_{act}), ion binding energy (E_b) and stabilization energy (E_s) of the ion pairs of the samples and fitting parameters determined from mobility plot using a VFT equation. The values of χ^2 parameters, represent the sum of the squared deviations between experimental values and theoretical values obtained from the fit.

Membrane	E_{act} (kJ·mol^{-1})	E_b (kJ·mol^{-1})	E_s (kJ·mol^{-1})	ln μ_∞ (m^2 V^{-1} s^{-1})	B (K)	T_0 (K)	χ^2
PBI@BMIN–NTf_2	10.9±0.3	12.3±0.5	1.4±0.8	-10.5±0.5	11.8±0.3	283±3	2.7×10^{-7}
PBI@BMIN–Cl	12.6±0.5	18.4±1.1	6.2±1.6	-9.5±0.4	159±11	255±3	0.00041
PBI@BMIN–BF_4	18.5±0.5	110±12	92±12	–9.2±0.3	703±13	175±2	0.0027
PBI@BMIN–NCS	25.1±1.2	148±15	123±16	–12.1±0.3	301±12	240±1.5	0.00053

A close inspection of our results shows that our anionic ILs have different mobility's depending of type of anion. These results permit us conclude that, long range forces induced by ILs may have an origin which can be related with the thickness of the diffuse electric double layer forces established when the Debye length arises from electrode polarization when the system reach the equilibrium. Other tentative explanation is based on the potential barrier that the anion must overcome to move from one ion pair to the next. When the amount of anions increases, the distance between neighboring ion pairs decreases and their Coulomb potential barrier increasingly overlaps, and therefore, decreasing the requested energy to produce a jump following the hopping mechanism and then increasing the mobility. A similar mechanism have been proposed by other researchers to explain the increasing in conductivity of different polymer salt electrolytes and in PPO/salt systems.[48,70]

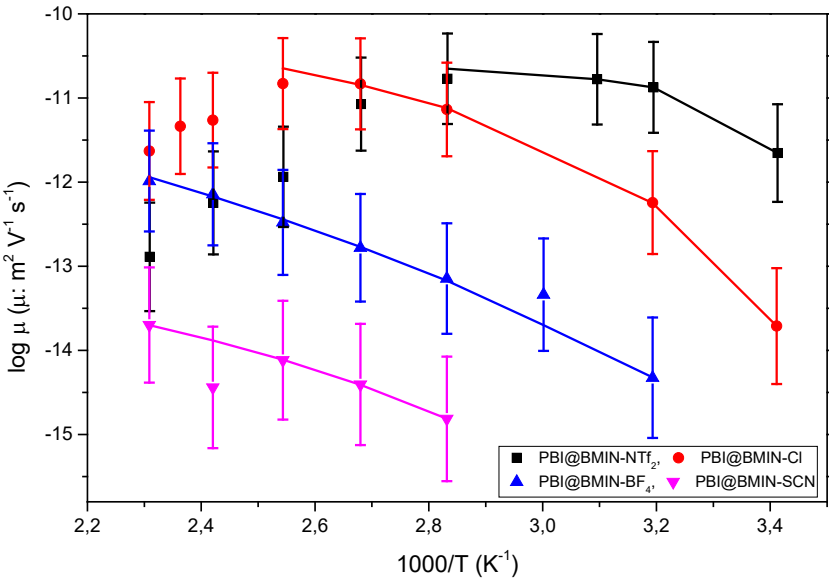

Figure 8. Temperature dependence of mobility for the different anions ionic liquids composite polybenzimidazol membranes.

Finally, from Eq.(9) we have obtained the mobile charge density. Our results show that the calculated charge concentration slightly varies with temperature (around one order of magnitude between 20 and 160 ºC), varying for the four films (**see Figure S5, Supporting Information**). For the PBI@BMIM–Cl membrane the calculated values are in the order of 10^{27} and 10^{28} m^{-3}, but rather surprisingly, the concentration is lower for the other films (from 10^{26} to 10^{27} m^{-3}). These values, calculated using the EP model, are higher than those from stoichiometric calculations where the concentration was calculated considering the IL composition in the membrane (0.05 g of IL in 1g of PBI) and the PBI density (1.7 g/cm3). For such composition the mobile charge density obtained was between $1.0–2.5\times10^{26}$ m^{-3}, yielding a dissociation degree of roughly 10^{-2} at 20 ºC. These values are quite similar to those found for other polyelectrolytes like a Li^+ poly(ethyleneoxide)-based sulfonated ionomer. However, it seems that our analysis on carrier's density based on EP over estimates the effective dissociated ion density about of 100 times than the

stoichiometric concentration, as similarly observed for other polymeric membranes containing ILs.[70,71,72]

Given the disparity in the obtained values of diffusivity (D) using the electrode polarization analysis, a correction considering the stoichiometric free-ion number density (n^*), should be introduced to give a corrected diffusivity D^*, as generally the number density of free ions, n^*, is considered to be constant at any temperature. Comparing the obtained values using Equations 6 and 9 for the calculation of the diffusivity and charge carriers density with the stoichiometric free ion number density; we obtain that the relationship between diffusivities and mobile charge density are given by $\frac{D}{D^*} = \frac{n^*}{n}$. Therefore, a correction on diffusivity by a factor of n^*/n needs should be considered when using the electrode polarization analysis of ionic mobility, as the dissociation-association dynamics should be assumed much faster than the macroscopic electrode polarization. These results suggest that the ionic transport in polymer composites containing Il's can be strongly decoupled from structural relaxation especially when the polymer had relatively rigid structures. On the other hand, the limitation of electrode polarization model might also be related to the structure of the double layer and the charge density distribution in membranes in the equilibrium under a dc parallel-plate field, where in the case of composite membranes containing liquid ionic the bulk permittivity might play an important role and where the Debye length can play an important role with the effective dissociation energy.

CONCLUSIONS

The incorporation of ILs into PBI polymeric matrices allows the fabrication of composite materials with excellent properties and potential applications for conductive membranes,

with no leaching of the liquid phase observed after long term experiments. We observed that conductivity of the different membranes studied increases with temperature and it depends on type of anion, reaching maximum values for PBI@BMIM–Cl and PBI@BMIM–NTf_2 (i.e. 1.0×10^{-4} S·cm^{-1} and 6.5×10^{-4} S·cm^{-1} at 160 ºC). Independently of temperature, the $[Cl]^-$ anion has the largest conductivity among the others anions under study. These conductivity values indicate that such composite materials represent a promising alternative with application in the design of different energy devices.

The diffusivity, mobility and charge carriers density, using the electrode polarization method have been determined for these PBI composite membranes. This formalism is very useful when the parameter loss tangent shows a maximum in the curves at each given temperature. Their corresponding values in frequency are related to the parameters *M,* τ_{EP} and α, and the diffusivity, mobility and charge carriers density were obtained. The diffusion coefficient and mobility of the ions follow a VFT temperature behavior with a good correlation. From the fits, the experimental ion-pair activation energy was found to be 10.9 ± 0.6 kJ·mol^{-1} for $[NTf_2]^-$ and higher values of 12.6 ± 0.7, 18.5 ± 0.9 and 25.1 ± 1.3 kJ·mol^{-1} for $[Cl]^-$, $[BF_4]^-$ and $[SCN]^-$ anions, respectively. From the results obtained for the parameters fit the loss tangent we can conclude that the corresponding dielectric strength exhibits a strong dependence on the anion. The mobility is between two or three orders of magnitude higher when the anion is Cl and NTf2, respect the BF4 and NCS anions, respectively. These results are in agreement with the diffusivities and conductivities observed. It is possible due to the strong electrostatic interaction between ion pairs and mobile anions assuming the formation of transient pairs in the case of BF_4 and NCS anions producing a diminution of carrier charge density into the polymeric matrix for PBI@BMIN–BF_4 and PBI@BMIN–NCS. This behavior could be related with the effective Debye length which values varying notably in composite

membranes containing ionic liquids and in particular, our results show that PBI@BMIN–BF_4 and PBI@BMIN–NCS membranes have a Debye length comprised around 1-2 nm in all the range of temperatures, while for PBI@BMIN–NTf_2 and PBI@BMIN–Cl Debye lengths are varying between 1000 nm and 10 nm from 20ºC to 160ºC, respectively.

AUTHOR INFORMATION

Corresponding Author

* E-mail: vicommo@ter.upv.es

ORCID

Jorge Escorihuela: 0000-0001-6756-0991

Vicente Compañ: 0000-0001-8233-7472

Author Contributions

The manuscript was written through contributions of all authors. All authors have given approval to the final version of the manuscript.

Funding Sources

This work was financially supported by the Ministerio de Economía y Competitividad (MINECO) under project ENE/2015-69203-R.

Conflicts of interest

There are no conflicts to declare.

REFERENCES

1 Steele, B. C. H.; Heinzel, A. Materials for fuel-cell technologies. *Nature* **2001**, *414*, 345–352.

2 Kreuer, K. D.; Portale, G. A critical revision of the nano-morphology of proton conducting ionomers and polyelectrolytes for fuel cell applications. *Adv. Funct. Mater*. **2013**, *23*, 5390−5397.

3 Bakangura, E.; Wu, L.; Ge, L.; Yang, Z.; Xu, T. Mixed matrix proton exchange membranes for fuel cells: State of the art and perspectives. *Prog. Polym. Sci*. **2016**, *57*, 103–152.

4. Armand M.; Chabagno, J. M.; Duclot M. Polyethers as solid electrolytes. In: Vashishta P.; Mundy J.N.; Shenoy G.K., Ed. Fast ion transport in solids: electrodes and electrolytes. North Holland Publishers, Amsterdan, 1979.

5 Di Noto, V.; Lavina, S.; Giffin, G. A.; Negro, E.; Scrosati, B. Polymer electrolytes: Present, past and future. *Electrochimica Acta* **2011**, *57*, 4–13.

6 Tarascon J.-M.; Armand, M. Issues and challenges facing rechargeable lithium batteries. *Nature* **2001**, *414*, 359–367.

7 Kraytsberg, A.; Ein-Eli, Y. Review of advanced materials for proton exchange membrane fuel cells. *Energy Fuels* **2014**, *28*, 7303–7330.

8 Reinholdt, M. X.; Kaliaguine, S. Proton exchange membranes for application in fuel cells: grafted silica/SPEEK nanocomposite elaboration and characterization. *Langmuir*, **2010**, *26*, 11184–11195.

9 Araya, S. S.; Zhou, F.; Liso, V.; Sahlin, S. L.; Vang, J. R.; Thomas, S.; Gao, X.; Jeppesen, C.; Kaer, S. K. A comprehensive review of PBI-based high temperature PEM fuel cells. *Int. J. Hydrogen Energy* **2016**, *41*, 21310–21344.

10 Ghosh, S.; Maity, S.; Jana, T. Polybenzimidazole/silica nanocomposites: Organic-inorganic hybrid membranes for PEM fuel cell. *J. Mater. Chem*. **2011**, *21*, 14897–14906.

11 Escorihuela, J.; García-Bernabé, A.; Montero, A.; Andrio, A.; Sahuquillo, O.; Giménez, E.; Compañ, V. Proton conductivity through polybenzimidazole composite membranes containing silica nanofiber mats. *Polymers* **2019**, *11*, 1182.

12 Fuentes, I.; Andrio, A.; Garcia-Bernabé, A.; Escorihuela, J.; Viñas, C.; Teixidor, F.; Compañ, V. Structural and dielectric properties of cobaltacarborane composite polybenzimidazole membranes as solid polymer electrolytes at high temperature. *Phys. Chem. Chem. Phys*. **2018**, *20*, 10173–10184.

13 Ozdemir, Y.; Uregen, N.; Devrim, Y. Polybenzimidazole based nanocomposite membranes with enhanced proton conductivity for high temperature PEM fuel cells. *Int. J. Hydrogen Energy* **2017**, *42*, 2648–2657.

14 Uregen, N.; Pehlivanoglu, K.; Ozdemir, Y.; Devrim, Y. Development of polybenzimidazole/graphene oxide composite membranes for high temperature PEM fuel cells. *Int. J. Hydrogen Energy* **2017**, *42*, 2636–2647.

15 Reyes-Rodriguez, J. L.; Escorihuela, J.; Garcia-Bernabé, A.; Giménez, E.; Solorza-Feria, O.; Compañ, V. Proton conducting electrospun sulfonated polyether ether ketone graphene oxide composite membranes. *RSC Adv*. **2017**, *7*, 53481–53491.

16 Escorihuela, J.; Sahuquillo, O.; García-Bernabé, A.; Giménez, E.; Compañ, V. Phosphoric acid doped polybenzimidazole (PBI)/zeolitic imidazolate framework composite membranes with significantly enhanced proton conductivity under low humidity conditions. *Nanomaterials* **2018**, *8*, 775.

17 Barjola, A.; Escorihuela, J.; Andrio, A.; Giménez, E.; Compañ, V. Enhanced conductivity of composite membranes based on sulfonated poly(ether ether ketone) (SPEEK) with zeolitic imidazolate frameworks (ZIFs). *Nanomaterials* **2018**, *8*, 1042.

18 Escorihuela, J.; Narducci, R.; Compañ, V.; Costantino, F. Proton conductivity of composite polyelectrolyte membranes with metal-organic frameworks for fuel cell applications. *Adv. Mater. Interfaces* **2019**, *6*, 1801146.

19 Liu, S.; Zhou, L.; Wang, P.; Zhang, F.; Yu, S.; Shao, Z.; Yi, B. Ionic-liquid-based proton conducting membranes for anhydrous H_2/Cl_2 fuel-cell applications. *ACS Appl. Mater. Interfaces* **2014**, *6*, 3195−3200

20 Kallem, P.; Eguizabal, A.; Mallada, R.; Pina, M. P. Constructing straight polyionic liquid microchannels for fast anhydrous proton transport. *ACS Appl. Mater. Interfaces* **2016**, *8*, 35377–35389.

21 Kallem, P.; Drobek, M.; Julbe, A.; Vriezekolk, E. J.; Mallada, R.; Pina, M. P. Hierarchical porous polybenzimidazole microsieves: an efficient architecture for anhydrous proton transport via polyionic liquids. *ACS Appl. Mater. Interfaces* **2017**, *9*, 14844−14857

22 Earle, M. J.; Seddon, K. R. Ionic liquids. Green solvents for the future. *Pure Appl. Chem*. **2000**, *72*, 1391–1398.

23. Plechkova, N. V.; Seddon, K. R. Applications of ionic liquids in the chemical industry. *Chem. Soc. Rev*. **2008**, *37*, 123–150.

24 Rehman, A.; Zeng, X. Ionic Liquids as green solvents and electrolytes for robust chemical sensor development. *Acc. Chem. Res*. **2012**, *45*, 1667–1677.

25 Qureshi, Z. S.; Deshmukh, K. M.; Bhanage, B. M. Applications of ionic liquids in organic synthesis and catalysis. *Clean Technol. Environ*. *Policy* **2014**, *16*, 1487−1513.

26 Ventura, S. P.; e Silva, F. A.; Quental, M. V.; Mondal, D.; Freire, M. G.; Coutinho, J. A. P. Ionic-liquid-mediated extraction and separation processes for bioactive compounds: past, present, and future trends. *Chem. Rev*. **2017**, *117*, 6984–7052.

27 González-Mendoza, L.; Altava, B.; Burguete, M. I.; Escorihuela, J.; Hernando, E.; Luis, S. V.; Quesada, R.; Vicent, C. Bis(imidazolium) salts derived from amino acids as receptors and transport agents for chloride anions. *RSC Advances* **2015**, *5*, 34415–34423.

28 Dai, C.; Zhang, J.; Huang, C.; Lei, Z. Ionic liquids in selective oxidation: catalysts and solvents. *Chem. Rev*. **2017**, *117*, 6929–6983.

29 González, L.; Escorihuela, J.; Altava, B.; Burguete, M. I.; Luis, S. V. Chiral room temperature ionic liquids as enantioselective promoters for the asymmetric aldol reaction. *Eur. J. Org. Chem*. **2014**, 5356–5363.

30 Lu, F.; Gao, X.; Wu, A.; Sun, N.; Shi, L.; Zheng, L. Lithium-containing zwitterionic poly(ionic liquid)s as polymer electrolytes for lithium-ion batteries. *J. Phys. Chem. C* **2017**, *121*, 17756–17763.

31 Quinn, B. M.; Ding, Z.; Moulton, R.; Bard, A. J. Novel electrochemical studies of ionic liquids. *Langmuir* **2002**, *18*, 1734–1742.

32 Santos, M. C. G.; Silva, G. G.; Santamaría, R.; Ortega, P. F. R.; Lavall, R. L. Discussion on operational voltage and efficiencies of ionic-liquid-based electrochemical capacitors. *J. Phys. Chem. C* **2019**, *123*, 8541–8549.

33 Watanabe, M.; Thomas, M. L.; Zhang, S.; Ueno, K.; Yasuda, T.; Dokko, K. Application of ionic liquids to energy storage and conversion materials and devices. *Chem. Rev*. **2017**, *117*, 7190–7239.

34 Dechnik, J.; Gascon, J.; Doonan, C. J.; Janiak, C.; Sumby, C. J. Mixed-matrix membranes. *Angew. Chem. Int. Ed*. **2017**, *56*, 9292–9310.

35 Rewar, A. S.; Chaudhari, H. D.; Illathvalappil, R.; Sreekumar, K.; Kharul, U. K. New approach of blending polymeric ionic liquid with polybenzimidazole (PBI) for enhancing physical and electrochemical properties. *J. Mater. Chem. A* **2014**, *2*, 14449-14458.

36 van de Ven, E.; Chairuna, A.; Merle, G.; Pacheco Benito, S.; Borneman, Z.; Nijmeijer, K. Ionic liquid doped polybenzimidazole membranes for high temperature Proton Exchange Membrane fuel cell applications. *J. Power Sources* **2013**, *222*, 202–209.

37 Mamlouk, M.; Ocon, P.; Scott, K. Preparation and characterization of polybenzimidzaole/diethylamine hydrogen sulphate for medium temperature proton exchange membrane fuel cells. *J. Power Sources* **2014**, *245*, 915–926.

38 Beltrán-Pitarch, B.; Prado-Gonjal, J.; Powell, A. V.; Martínez-Julián, F.; García-Cañadas, J. Complete characterization of thermoelectric materials by impedance spectroscopy. *J. Phys. Chem. C* **2019**, *123*, 12608−12613.

39 Trukhan. E. M. Dispersion of the dielectric constant of heterogeneous systems. *Sov. Phys. Solid. State* **1963**, *4*, 2560–2570.

40 Macdonald, J. R. Theory of AC space-charge polarization effects in photoconductors, semiconductors, and electrolytes. *Phys. Rev.* **1953**, *92*, 4–17.

41 Macdonald, J. R. Utility of continuum diffusion models for analyzing mobile-ion immittance data: electrode polarization, bulk, and generation–recombination effects. *J. Phys. Condens. Mater*. **2010**, *22*, 495101.

42 Macdonald, J. R. Evangelista, I. R.; Enzi, E. K.; Barbero, G. Comparison of impedance spectroscopy expressions and responses of alternate anomalous Poisson−Nernst−Planck diffusion equations for finite-length situations. *J. Phys. Chem C*. **2011**, *115*, 7648–7655.

43 Coelho, R. Sur la relaxation d'une charge d'espace. *Rev. Phys. Appl.* **1983**, *18*, 137–146.

44 Coelho, R. On the static permittivity of dipolar and conductive media – an educational approach. *J. Non-Cryst. Solids* **1991**, *131*, 1136–1139.

45 Schütt, H. J.; Gerdes, E. Space-charge relaxation in ionicly conducting oxide glasses. I. Model and frequency response. *J. Non-Cryst. Solids* **1992**, *144*, 1–13.

46 Schütt, H. J.; Gerdes, E. Space-charge relaxation in ionicly conducting glasses. II. Free carrier concentration and mobility. *J. Non-Cryst. Solids* **1992**, *144*, 14–20.

47 Sørensen, T. S.; Compañ, V.; Diaz-Calleja, R. Complex permittivity of a film of poly [4-(acryloxy)phenyl-(4-chlorophenyl)methanone] containing free ion impurities and the separation of the contributions from interfacial polarization, Maxwell-Wagner-Sillars effects and dielectric relaxations of the polymer chains. *J. Chem. Soc., Faraday Trans.* **1996**, *92*, 1947–1957.

48 Fragiadakis, D.; Dou, S.; Colby, R. H.; Runt, J. Molecular mobility and Li+ conduction in polyester copolymer ionomers based on poly(ethylene oxide). *J. Chem. Phys.* **2009**, *130*, 064907.

49 Bandara, T. M. W. J.; Dissanayake, M. A. K. L.; Albinsson, I.; Mellander, B.-E. Mobile charge carrier concentration and mobility of a polymer electrolyte containing PEO and Pr_4N^+ I^- using electrical and dielectric measurements. *Solid State Ionics* **2011**, *189*, 63–68.

50 Baur, J. E. In Handbook of Electrochemistry; Zoski, C. G., Ed.; Elsevier Science, 2007; p. 829-848.

51 Sangoro, J. R.; Serghei, A.; Naumov, S.; Galvosas, P.; Kärger, J.; Wespe, C.; Bordusa, F.; Kremer, F. Charge transport and mass transport in imidazolium-based ionic liquids. *Phys. Rev. E* **2008**, *77*, 051202.

52 Serghei, A.; Tress, M.; Sangoro, J. R.; Kremer, F. Electrode polarization and charge transport at solid interfaces. Phys. Rev. B 2009, 80, 184301.

53 Sangoro, J.; Iacob, C.; Serghei, A.; Naumov, S.; Galvosas, P.; Karger, J.; Wespe, C.; Bordusa, F.; Stoppa, A.; Hunger, J.; Buchner, R.; Kremer, F. Decoupling of ionic conductivity from structural dynamics in polymerized ionic liquids. *Soft. Matter*. **2014**, *10*, 3536–3540.

54 Mauritz, K. A. Dielectric relaxation studies of ion motions in electrolyte-containing perfluorosulfonate ionomers. 4. Long-range ion transport. *Macromolecules* **1989**, *22*, 4483–4488.

55 Wübbenhorst, M.; van Turnhout, J. Analysis of complex dielectric spectra. I. One-dimensional derivative techniques and three-dimensional modelling. *J. Non-Cryst. Solids* **2002**, *305*, 40–49.

56 Colomban, P.; Badot, J. C. Radiowave and microwave frequency dielectric relaxations at the superionic, incommensurate and ferroelectric phase transitions in NH_4HSeO_4 and ND_4DSeO, *J. Phys.: Condens. Mater.* **1992**, *4*, 5625–5638.

57 Escorihuela, J.; García-Bernabé, A.; Montero, A.; Sahuquillo, O.; Giménez, E.; Compañ, V. Ionic liquid composite polybenzimidazol membranes for high temperature PEMFC applications. Polymers 2019, 11, 732

58 The oxidative stability of the membranes was investigated by immersing the membranes in Fenton's reagent (3% H_2O_2 solution containing 4 ppm Fe^{2+}) at 70 °C. The samples were collected by filtering and rinsed with deionized water several times, then dried at 120 °C for 5 h in a vacuum oven. Next, the degradation of the membranes was evaluated by their weight loss.

59 Nyquist, H. Thermal agitation of electric charge in conductors. *Phys. Rev*. **1928**, *32*, 110.

60 Schröder, C; Rudas, T.; Steinhauser, O. Simulation studies of ionic liquids: Orientational correlations and static dielectric properties. J. Chem. Phys. **2006**, *125*, 244506.

61 Tsuzuki, S.; Tokuda, H.; Hayamizu, K.; Watanabe, M. Magnitude and Directionality of Interaction in Ion Pairs of Ionic Liquids: Relationship with Ionic Conductivity. *J. Phys Chem B*, **2005**, *109*, 16474–16481

62 Becke, A. D. Density-functional thermochemistry. III. The role of exact exchange. *J. Chem. Phys.* **1993**, *98*, 5648–5652.

63 Gaussian 16, Revision B.01, Frisch, M. J. et al. Gaussian, Inc., Wallingford CT, 2016 (see Supporting Information for full Gaussian citation).

64 Gebbie, M. A.; Smith, A. M.; Dobbs, H. A.; Lee, A. A.; Warr, G. G.; Banquy, X.; Valtiner, M.; Rutland, M. W.; Israelachvili, J. N.; Susan Perkin, S.; Atkin, R. Long range electrostatic forces in ionic liquids. *Chem. Commun*. **2017**, *53*, 1214–1224.

65 Weingärtner, H. Understanding ionic liquids at the molecular level: facts, problems, and controversies. *Angew. Chem. Int. Ed*. **2008**, *47*, 654–670.

66 Kuriakose, M.; Longuemart, S.; Depriester, M.; Delenclos, S.; Hadj Sahraoui, A. Maxwell-Wagner-Sillars effects on the thermal-transport properties of polymer-dispersed liquid crystals. *Phys. Rev. E*. **2014**, *89*, 022511.

67 Samet, M.; Levchenko, V.; Boiteux, G.; Seytre, G.; Kallel, A.; Serghei, A. Electrode polarization vs. Maxwell-Wagner-Sillars interfacial polarization in dielectric spectra of materials: Characteristic frequencies and scaling laws. *J. Chem. Phys.* **2015**, *142*, 194703.

68 Wang, Y.; Sun, C.-N.; Fan, F.; Sangoro, J. R.; Berman, M. B.; Grenbaum, S. G.; Zawodzinski, T. A.; Sokolov, A. P. Examination of methods to determine free-ion

diffusivity and number density from analysis of electrode polarization. *Phys. Rev. E*. **2013**, *87*, 042308.

69 Klein, R. J.; Zhang, S.; Dou, S.; Jones, B. H.; Colby, R. H.; Runt, J. Modeling electrode polarization in dielectric spectroscopy: Ion mobility and mobile ion concentration of single-ion polymer electrolytes. *J. Chem. Phys.* **2006**, *124*, 144903.

70 Bruce P. G.; Gray, F. M. In Solid State Electrochemistry, Bruce P. G., Ed. Cambridge University Press, Cambridge, 1995.

71 Valverde, D.; Garcia-Bernabé, A.; Andrio, A.; García-Verdugo, E.; Luis, S. V.; Compañ, V. Free ion diffusivity and charge concentration on cross-linked polymeric ionic liquid iongel films based on sulfonated zwitterionic salts and lithium ions. *Phys. Chem. Chem. Phys*. **2019**, *21*, 17923–17932.

72 Fragiadakis, D.; Dou, S.; Colby, R. H.; Runt, J. Molecular mobility, ion mobility, and mobile ion concentration in poly(ethylene oxide)-based polyurethane ionomers. *Macromolecules* **2008**, *41*, 5723–5728.